CARBON 50 (2012) 1051–1056

Available at www.sciencedirect.com

SciVerse ScienceDirect

journal homepage: www.elsevier.com/locate/carbon

Characterization of activated carbon fiber/polyaniline materials by position-resolved microbeam small-angle X-ray scattering

D. Salinas-Torres [a], J.M. Sieben [b], D. Lozano-Castello [a], E. Morallón [b], M. Burghammer [c], C. Riekel [c], D. Cazorla-Amorós [a,*]

[a] Departamento de Química Inorgánica and Instituto Universitario de Materiales, Universidad de Alicante, Ap. 99, E-03080, Spain
[b] Departamento de Química Física and Instituto Universitario de Materiales, Universidad de Alicante, Ap. 99, E-03080, Spain
[c] European Synchrotron Radiation Facility, Grenoble, France

ARTICLE INFO

Article history:
Received 21 July 2011
Accepted 6 October 2011
Available online 14 October 2011

ABSTRACT

Activated carbon fiber (ACF)/polyaniline (PANI) materials have been prepared using two different methods, viz. chemical and electrochemical polymerization. Electrochemical characterization of both materials shows that the electrodes with polyaniline have a higher capacitance than does a pristine porous carbon electrode. To analyze the distribution of PANI within the ACF, characterization by position-resolved microbeam small-angle X-ray scattering (μSAXS) has been carried out. μSAXS results obtained with a single ACF indicate that, for the experimental conditions used, a PANI coating is formed inside the micropores and that it is higher in the external regions of the ACF than in the core. Additionally, it seems that the penetration of PANI inside the fibers occurs in a larger extent for the chemical polymerization or, in other words, for the electrochemically polymerized sample there is a slightly larger accumulation of PANI in the external regions of the ACF.

1. Introduction

Conducting polymer-based materials is a subject of a strong research because of their wide range of applications. Thus, development of electrodes for sensors, batteries, capacitors, electrocatalyst support and corrosion protection are examples that show the interest of this kind of materials [1,2]. One of the aspects in which researchers pay more attention is the synthesis stage, where the preparation of thin films of the conducting polymer on a given support is probably one of the key objectives.

Among the conducting polymers, polyaniline (PANI), which is an amorphous polymer, has gained increasing attention because of different interesting properties such as, easy polymerization in aqueous media, good stability in air, low cost production, relatively high conductivity and high pseudocapacitance for thin films [3–10]. However, one of the limitations of PANI is the poor mechanical properties due to changes in volume of the PANI amorphous film upon doping and de-doping, what results in a poor cycling life. One possibility to solve this limitation is the preparation of PANI-based materials in which a thin film of the conducting polymer is deposited on an appropriate high surface area support [10–12].

For the specific application in supercapacitors, the use of different carbon materials as support and different polymerization methods, have been studied. The preparation method of the PANI film, for example chemical or electrochemical polymerization, has a strong effect on the final properties of the film [9,10], although the surface chemistry of the support may also play an important role [9].

* *Corresponding author:* Fax: +34 965903454.
E-mail address: cazorla@ua.es (D. Cazorla-Amorós).
0008-6223/$ - see front matter
doi:10.1016/j.carbon.2011.10.010

In this work, we contribute to this subject by presenting unique experiments obtained by small angle X-ray scattering with a microbeam (μSAXS) of carbon/PANI materials (in this case we have used activated carbon fibers – ACF). This technique has been successfully applied by our research group to characterize the porosity of ACF across the fiber diameter [13–16]. The use of a micrometer size beam and a high precision scanning system gives the possibility of detecting local heterogeneities such as skin/core differentiation, open and closed porosity and orientation of scattering objects, among others [17,18]. Then, this technique is very powerful and convenient to explore how the polymer layer is distributed across the fiber diameter and may provide very useful information on the position-resolved distribution of PANI films inside the porosity of the porous carbon depending on the polymerization method used.

2. Experimental

2.1. Samples preparation

ACF/PANI electrodes were prepared using a commercial ACF (A20; Osaka Gas Co. Ltd.) and carrying out a polymerization of aniline. Two different polymerization methods were used:

(i) Chemical polymerization (sample A20_C): previous to the polymerization, the adsorption isotherm in aniline solution on the ACF was obtained. Then, the conditions selected for the preparation of the ACF/PANI material corresponds to a loading of 30 wt.% of aniline in the final sample according to the aniline isotherm obtained with the A20. The A20 loaded with PANI was prepared by introducing 600 mg of A20 during 24 h in a 0.02 M aniline solution. After aniline adsorption, the sample was introduced for an hour in an ammonium persulphate solution in 1 M HCl. The oxidant amount was calculated in order to obtain an aniline:ammonium persulphate molar ratio equal to 1:1. A polyaniline coating is then obtained over the carbon material. The resulting A20/PANI material was washed with 1 M HCl, followed by washing with 1 M NH_4OH. The material was dried in dynamic vacuum for 24 h. For the electrode preparation, the A20/PANI material has been mixed with the binder polytetrafluoroethylene (PTFE, 60 wt.%) and acetylene black (Strem Chemicals) in a ratio 80:10:10 wt.%. The total electrode weight used for the measurements was about 40 mg.

(ii) Electrochemical polymerization (sample A20_E): the procedure used is that described in Ref. [10]. This method consists in mixing a paste of the A20 (~3 mg) with the binder (PTFE, 60 wt.%) and the conductivity promoter (acetylene black) in a ratio 80:10:10 wt.%; this mixture was spread and pressed uniformly and thinly with a spatula onto a graphite disk electrode (0.6 cm diameter). After drying, the electrode was placed as the working electrode in a solution of 0.15 M aniline + 1.0 M HCl + 0.5 M KCl and subjected to electropolymerization using a three electrodes electrochemical cell. A platinum wire was used as counter electrode and a reversible hydrogen electrode (RHE) served as reference electrode. Single potential step from the lower potential of 0.3 V, where no electrode reaction occurred, to an upper potential of 1.05 V, where the polymerization took place, was done for a time until the total charge passed was 0.50 C mg^{-1}. The amount of polyaniline was calculated by subtracting the total weight after polymerization to the mass of carbon material. The amount of PANI loaded was around 30 wt.%.

For the characterization of the sample without polyaniline, the electrode was prepared from A20 material, acetylene black (Strem Chemicals) and binder in a ratio 80:10:10 wt.%, respectively. The total electrode weight used for the measurements was about 40 mg. After that, the electrode was placed in a stainless steel mesh as a current collector.

2.2. Characterization

The characterization of the porosity of the A20 was done using physical adsorption of N_2 at 77 K and CO_2 at 273 K (Quantachrome, Autosorb-6). The samples were outgassed at 523 K under vacuum for 4 h. Nitrogen adsorption results were used to determine BET surface area values and Dubinin–Radushkevich (DR) micropore volumes (V_{DR} N_2) as well as the average pore size [19,20]. Narrow micropore volume (pore size <0.7 nm, approximately) was obtained from CO_2 adsorption data (V_{DR} CO_2) [20]. Table 1 shows the porous texture values obtained for the activated carbon fibers.

Scattering experiments were carried out at the microfocus beamline (ID13) in the European Synchrotron Radiation Facility (ESRF) in Grenoble, France. The beam selected for the experiments of this study was a 0.5 μm beam produced by Kirkpatrick–Baez mirrors (wavelength $\lambda = 0.975$ Å). The domain of q values investigated with this setup ranging from 0.2 nm^{-1} to 3 nm^{-1}. An area detector (MAR-CCD) with an active diameter of 130 mm was used for the measurements. The distance from the detector to the samples was 470 mm. These μSAXS measurements were carried out scanning the fiber across its diameter with a step size of 1 μm and with accuracy between 0.1 μm and 0.5 μm. The samples were previously embedded in a resin for facilitating the posterior cut for the analysis. The experiments were done on thin microtome cross-sections (films of about 10 μm thickness). Each sample was scanned horizontally and vertically. All measured data were corrected for background. A view of the experimental set-up can be found elsewhere [17]. Data evaluation was done using the software package FIT2D [21]. Several microtome cross-sections of a given sample were measured and similar scattering intensities were obtained. Additionally, the scattering intensity is similar to a non-embedded ACF

Table 1 – Porous texture characterization of the pristine activated carbon fibers.

Sample	BET (m^2 g^{-1})	V_{DR} N_2 (cm^3 g^{-1})	V_{DR} CO_2 (cm^3 g^{-1})
A20	1660	0.78	0.38

sample. This indicates that the resin does not penetrate inside the microporosity of the ACF, what is reasonable considering the viscosity of the resin and the short contact time used.

The electrochemical characterization of the electrodes was done using a standard three electrodes cell configuration. Reversible hydrogen electrode (RHE), immersed in the same solution, was used as reference and a spiral of platinum wire was employed as a counter electrode. 0.5 M H_2SO_4 was used as aqueous electrolyte.

The electrochemical behavior of the samples was assessed by cyclic voltammetry at 1 mV s^{-1} and galvanostatic method. The capacitance values were calculated from the interval between 0.2 V and 0.6 V, dividing the imposed current (60 mA g^{-1}) by the slope of the lineal chronopotentiograms plot, taking the average value between charge and discharge processes. The result is expressed in F g^{-1} taking into account the weight of the active part of the electrode, that is, A20 and polyaniline.

All electrochemical measurements were carried out with an EG&G Potentionstat/Galvanostat model 273 controlled by software ECHEM M270. All the solutions were prepared with ultrapure water (Purelab ELGA) with a resistivity of 18 MΩ cm.

3. Results and discussion

3.1. *Electrochemical characterization*

Fig. 1 shows the cyclic voltammograms at a slow scan rate (1 mV s^{-1}) of pristine A20 and the A20/PANI electrodes prepared by chemical and electrochemical polymerization of aniline on the activated carbon fibers, respectively. The carbon material presents a quasi-rectangular shape, indicating that the main contribution to capacitance is the charge and discharge of the double layer. A redox process is observed around 0.56 V during the positive sweep that corresponds to the surface oxygen groups on the carbon material [22]. However, the materials in presence of polyaniline present several overlapped peaks, indicating the contribution of redox processes produced by the polyaniline. It is interesting to note that the cyclic voltammogram of the A20_E sample presents more pronounced peaks than in the case of chemical polymerization (A20_C).

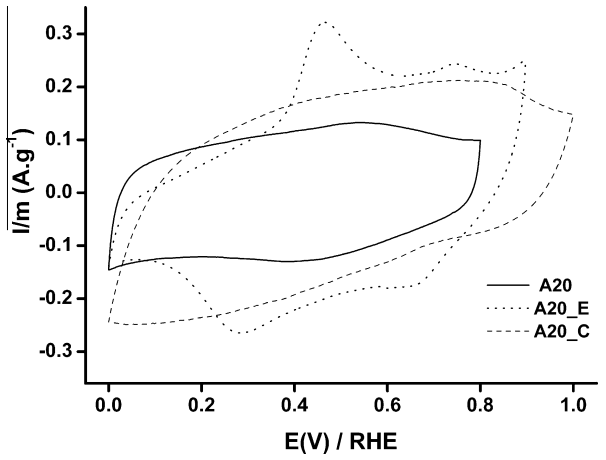

Fig. 1 – Steady state voltammograms obtained for the activated carbon fibers, A20 (– – –) and the A20/PANI samples A20_C (—) and A20_E (·····). 0.5 M H_2SO_4. v = 1 mV s^{-1}.

The anodic voltammetric peaks in Fig. 1 between 0.4 V and 0.5 V observed for the A20_E electrode can be related to the oxidation of the leucoemeraldine state to emeraldine state of polyaniline and the second peak between 0.7 V and 0.8 V to the benzoquinone–hydroquinone redox couple [10,23]. The latter process is produced by the degradation products of polyaniline during the synthesis [10,24]. It is well-known that the physical and chemical properties of PANI are influenced by the preparation method [25]. Then, in the voltammogram of the material prepared by chemical method the redox processes are less defined because in that case several by-products are formed. But, in the case of electrochemical polymerization, the polymer chains are larger than those from the chemical method, resulting in a polymer with less defects [25,26].

The activated carbon fiber/polyaniline electrodes prepared as described in Section 2 were characterized by chronopotentiometry. The samples were subjected to charge–discharge cycles by constant current of 60 mA g^{-1}. The results for the experiments are presented in Table 2. It can be observed that the capacitance increases for the A20/PANI materials in comparison to the pristine activated carbon fiber as consequence of the pseudocapacitance contribution of PANI. Additionally, it can be observed that the increase in capacitance in the PANI containing electrodes is similar for both preparation methods, in agreement with the similar amount of conducting polymer of both materials.

3.2. *Characterization of A20 and A20/PANI materials by μSAXS*

Fig. 2 includes the two-dimensional scattering patterns corresponding to the measurements at the center of the fiber for the commercial A20 and the A20/PANI material prepared by chemical polymerization, as an example of the results observed for the A20/PANI materials. This figure shows that the scattering for the A20 is the same in all directions what indicates the isotropic distribution of pores around the fiber axis in this kind of materials and that there is no preferential orientation of the porosity created during the activation around the fiber axis.

This observation is similar to that obtained with A20 prepared by CO_2, steam, KOH or NaOH activations of isotropic carbon fibers [13,16]. The scattering pattern for the A20/PANI samples, still maintains such isotropic character but the scattering intensity decreases importantly, showing that the PANI is filling the porosity of the A20. This is in agreement with the

Table 2 – Specific capacitance obtained in a chronopotentiometric experiment at 60 mA g^{-1} in 0.5 M H_2SO_4 for the different samples.

Sample	Capacitance (F g^{-1})
A20	159
A20_C	233
A20_E	233

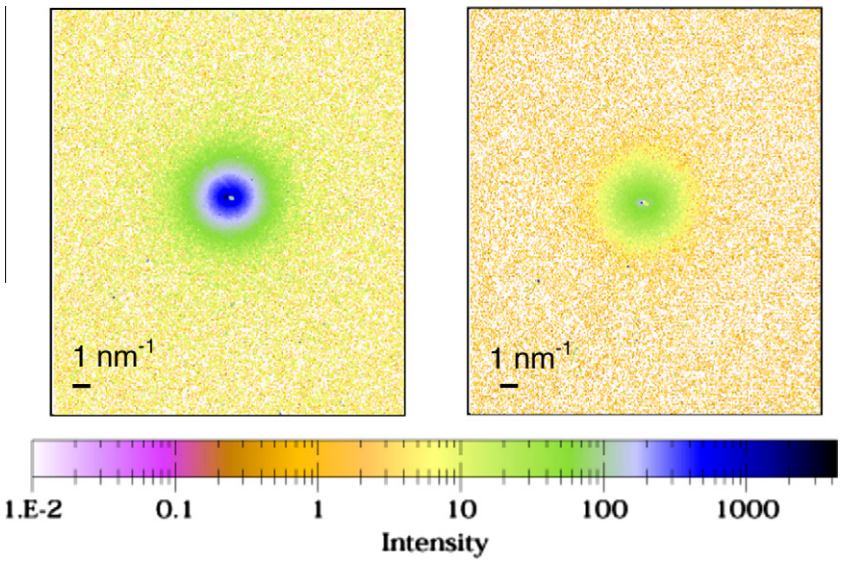

Fig. 2 – Two-dimensional scattering patterns obtained at the center of the fiber of the A20 sample (left) and the A20/PANI sample prepared using chemical polymerization method (A20_C) (right).

observed decrease in the micropore volume, measured by N_2 adsorption at 77 K, of the A20/PANI material prepared by chemical polymerization (which is the only one that can be measured because of the available amount of sample) with respect to the A20 (V_{DR} N_2 decreases from 0.78 for the pristine A20 to 0.43 $cm^3\ g^{-1}$ for the A20_C sample).

Fig. 3 includes the integrated scattering patterns for the original A20 and the two A20/PANI materials prepared using the two different polymerization processes (i.e., chemical and electrochemical methods) and measured at the center of the fibers. It is clearly seen that the intensity decreases for the A20/PANI samples compared to the starting A20 in the scattering region corresponding to micropores. Then, the results indicate that, for both methods, the deposition of polyaniline takes place inside the microporosity existing in the starting A20.

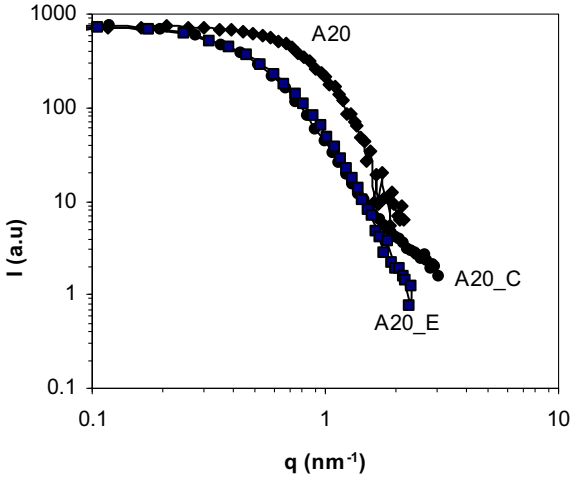

Fig. 3 – Scattering curves corresponding to measurements at the center of the fiber for the A20 and two A20/PANI samples prepared using two different methods (chemical (sample A20_C) and electrochemical (sample A20_E)).

From the integrated scattering patterns and assuming that the pores have a slit shape, an estimation of the pore size can be calculated considering that the scattering objects have a lamellar shape. Then, from a plot of $\ln(I\,q^2)$ vs q^2 in the region of $2\pi/S_t^{0.5} \leqslant q \leqslant 1/R_t$, R_t can be calculated (where S_t is the cross section of the lamella and R_t is the radius of gyration of the thickness of the lamella (T)) [27]. From the linear part of the plot, the slope ($-R_t^2$) is obtained and from it, the thickness of the pores can be estimated: $T = 12^{0.5}R_t$ [27,28].

Table 3 includes the average pore size for the three materials calculated with the above equation. Since no significant differences have been found at different positions of the A20, the average pore size has been calculated. The table also includes the average pore size calculated from the N_2 adsorption isotherms at 77 K by applying the DR equation for the pristine A20 and the A20/PANI material obtained by chemical polymerization. In these both cases, enough amount of sample is available to do the isotherms. Interestingly, the average pore sizes obtained from μSAXS and gas adsorption are similar in spite of the different theoretical and experimental approaches, what supports the validity of the analysis method used for the SAXS measurements. The results show that the average pore size of the A20 decreases about 1 nm upon addition of the PANI, being this decrease related to the PANI layers deposited on both walls of the slit shaped pores. This means that the average thickness of the PANI layer is close to 0.5 nm, a value which is similar to the thickness of a monolayer of

Table 3 – Estimated pore size for the pristine A20 and the A20/PANI samples, calculated from μSAXS data and from N_2 adsorption by applying the DR equation.

Sample	Pore size from μSAXS (nm)	Pore size from DR equation (nm)
A20	2.7	2.2
A20_C	1.6	1.8
A20_E	1.7	–

PANI [29]. Thus, the results suggest that, at the polymerization conditions used, a very thin layer of PANI is deposited over the surface of the pristine A20 sample. Considering that the external surface is negligible compared to the micropores surface, the PANI film is essentially located inside the slit shaped pores of the pristine A20. This result points out that the approaches and conditions used in the present work has allowed us to successfully obtain A20/PANI materials, which may fulfill the requirements for several application such as supercapacitors; i.e.: (i) deposition of PANI as a thin film over the support, to allow better redox kinetics; and (ii) PANI coating distribution inside the microporosity, so that the carbon material can provide better mechanical properties and high surface area.

In order to analyze the distribution of PANI in the A20, that is, to observe if the deposition of PANI is similar in all the regions across the fiber diameter, scattering measurements across the fiber diameter have been done. From the integrated scattering curves such as those in Fig. 3, a useful parameter for the analysis of porous materials, Porod Invariant (PI), has been obtained. PI is defined as [30]:

$$\mathrm{PI} = \int q^2 I(q) dq \quad (1)$$

PI is related to the void fraction (ϕ) of the material under investigation, as indicated in Eq. (2),

$$\frac{1}{V}\mathrm{PI} = 2\pi(\Delta\rho)^2\phi(1-\phi) \quad (2)$$

where ρ is the electronic density, $(\Delta\rho)^2$ is the contrast term and V is the sample volume. Thus, PI gives a useful comparison of how the void fraction of materials changes following upon PANI addition.

Fig. 4 includes the normalized Porod Invariant (PI) values estimated for the different measurements carried out across the fiber diameter versus the beam position for the starting A20 and for the two A20/PANI samples (chemical method (A20_C) and electrochemical method (A20_E)).

In the plot of Fig. 4, beam position equal to zero corresponds to the center of the fiber. Interestingly, the figure shows that the fiber diameter does not change in the A20/PANI materials compared to the original A20, indicating, once more, that the PANI film is homogeneously deposited over the surface of the fibers and that it is essentially inside the micropores. Additionally, the figure shows that the scattering profiles, as a function of the position of the fibers, are different for the two A20/PANI samples and the starting A20. In the case of the starting A20, the scattering is similar for all the regions, indicating a homogeneous distribution of porosity within the fibers. However, for the A20/PANI samples the scattering intensity is higher at the internal zones than at the external parts of the fibers, which seems to point out that, for both methods (chemical and electrochemical methods) the deposition of PANI is higher in the external regions of the fibers than in the core. Additionally, it seems that the penetration of PANI inside the micropores of the fibers occurs in a larger extent for the chemical polymerization, what can be in agreement with the larger contact time of the aniline with the A20 before the polymerization. It should be noted for clarity purposes that, in all the PANI containing samples, the scattering decreases compared to the pristine A20 (as discussed regarding Figs. 2 and 3) in all the measurements done at different positions.

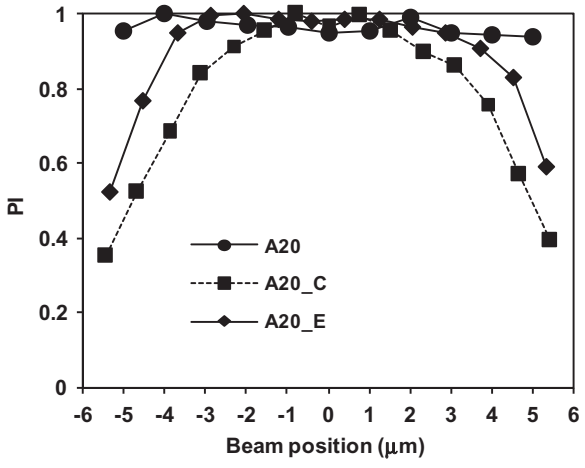

Fig. 4 – Normalized Porod Invariant values estimated for the different measurements carried out across the fiber diameters of the A20, A20_C and A20_E samples.

4. Conclusions

Position-resolved microbeam small angle X-ray scattering (μSAXS) measurements on A20/PANI materials point out that this technique is very powerful and convenient to explore how the polymer layer is distributed across the fiber diameter and have provided very useful information on the position-resolved distribution of PANI films inside the porosity of the A20 depending on the polymerization method used. The results reveal that, for both preparation methods (chemical and electrochemical polymerization) and at the experimental conditions used, a PANI coating is formed over the surface of the fibers, which is essentially inside the micropores, and that it is higher in the external regions of the A20 than in the core. The fiber diameter is not changed, and it seems that the penetration of PANI inside the fibers occurs in a larger extent for the chemical polymerization what is in agreement with the larger contact time of the aniline with the A20 before the polymerization.

This type of information provided by μSAXS is very interesting to further design and prepare A20/PANI materials for different applications such as supercapacitors.

Acknowledgments

The authors would like to thank the Spanish MICINN, FEDER and PLAN E funds (Project CTQ2009-10813/PPQ, MAT2010-15273 and PLE2009-0021), Generalitat Valenciana and FEDER (PROMETEO/2009/047) and ESRF (Grenoble, Experiment Number MA-365) for financial support. J.M. Sieben thanks the Spanish MEC for a mobility grant (SB2010-0132).

REFERENCES

[1] Snook GA, Kao P, Best AS. Conducting-polymer-based supercapacitor devices and electrodes. J Power Sources 2011;196(1):1–12.

[2] Skotheim TA, Elsenbaumer RL, Reynolds JR. Handbook of conducting polymers. New York: Marcel Dekker; 1998.
[3] Conway BE. Electrochemical supercapacitors: scientific fundamentals and technological applications. New York: Kluwer Academic/Plenum Publishers; 1999.
[4] Ryu KS, Kim KM, Park NG, Park YJ, Chang SH. Symmetric redox supercapacitor with conducting polyaniline electrodes. J Power Sources 2002;103(2):305–9.
[5] Ko JM, Song R, Yu HJ, Yoon JW, Min BG, Kim DW. Characteristics of supercapacitor electrodes of PBI-based carbon nanofiber web prepared by electrospinning. Electrochim Acta 2004;50(2–3):877–81.
[6] Mondal SK, Barai K, Munichandraiah N. High capacitance properties of polyaniline by electrochemical deposition on a porous carbon substrate. Electrochim Acta 2007;52(9):3257–8.
[7] Talbi H, Just PE, Dao LH. Electropolymerization of aniline on carbonized polyacrylonitrile aerogel electrodes: applications for supercapacitors. J Appl Electrochem 2003;33(6):465–73.
[8] Wu MQ, Snook GA, Gupta V, Shaffer M, Fray DJ, Chen GZ. Electrochemical fabrication and capacitance of composite films of carbon nanotubes and polyaniline. J Mater Chem 2005;15(23):2297–303.
[9] Bleda-Martinez MJ, Morallon E, Cazorla-Amoros D. Polyaniline/porous carbon electrodes by chemical polymerization: effect of carbon surface chemistry. Electrochim Acta 2007;52(15):4962–8.
[10] Bleda-Martínez MJ, Peng C, Zhang S, Chen GZ, Morallón E, Cazorla-Amorós D. Electrochemical methods to enhance the capacitance in activated carbon/polyaniline composites. J Electrochem Soc 2008;155(9):A672–8.
[11] Prasad KR, Munichandraiah NJ. Potentiodynamically deposited polyaniline on stainless steel. J Electrochem Soc 2002;149(11):A1393–9.
[12] Zhou H, Chen H, Luo SL, Lu GW, Wei WZ, Kuang YFJ. The effect of the polyaniline morphology on the performance of polyaniline supercapacitors. J Solid State Electr 2005;9(8):574–80.
[13] Lozano-Castelló D, Raymundo-Piñero E, Cazorla-Amorós D, Linares-Solano A, Müller M, Riekel C. Characterization of pore distribution in activated carbon fibers by microbeam small angle X-ray scattering. Carbon 2002;40:2727–35.
[14] Lozano-Castelló D, Raymundo-Piñero E, Cazorla-Amorós D, Linares-Solano A, Müller M, Riekel C. Microbeam small angle X-ray scattering (μSAXS): a novel technique for the characterization of activated carbon fibers. Stud Surf Sci Catal 2002;144:51–8.
[15] Lozano-Castelló D, Cazorla-Amorós D, Linares-Solano D. Microporous solid characterization: use of classical and "new" techniques. Chem Eng Technol 2003;26(8):852–7.
[16] Lozano-Castelló D, Maciá-Agulló JA, Cazorla-Amorós D, Linares-Solano A, Müller M, Burghammer M, et al. Isotropic and anisotropic microporosity development upon chemical activation of carbon fibers, revealed by microbeam small-angle X-ray scattering. Carbon 2006;44(7):1121–9.
[17] Riekel C, Burghammer M, Davies R, Gebhardt R, Popov D. Fundamentals of soft condensed matter scattering and diffraction with microfocus techniques. Lect Notes Phys 2009;776:91–104.
[18] Cazorla-Amoros D, Lozano-Castello D, Müller M. Application of non-crystalline diffraction with microfocus to carbon fibers. Lect Notes Phys 2009;776:199–216.
[19] Stoeckli F, Ballerini L. Evolution of microporosity during activation of carbon. Fuel 1991;70(4):557–9.
[20] Cazorla-Amoros D, Alcañiz-Monge J, de la Casa-Lillo MA, Linares-Solano A. CO_2 as an adsorptive to characterize carbon molecular sieves and activated carbons. Langmuir 1998;14(16):4589–96.
[21] Hammersley AP. ESRF Internal Report, ESRF97HA02T, FIT2D: an introduction and overview, 1997.
[22] Bleda-Martínez MJ, Lozano-Castelló D, Morallón E, Cazorla-Amorós D, Linares-Solano A. Chemical and electrochemical characterization of porous carbon materials. Carbon 2006;44(13):2642–51.
[23] Santiago EI, Pereira EC, Bulhoes LOS. Characterization of the redox processes in polyaniline using capacitance–potential curves. Synthetic Met 1998;98(2):87–93.
[24] Aoki K, Tano S. Simultaneous occurrence of polymerization and decomposition of polyaniline films. Electrochim Acta 2005;50(7–8):1491–6.
[25] Nekrasov AA, Ivanov VF, Gribkova OL, Vannikov AV. Electrochemical and chemical synthesis of polyaniline on the surface of vacuum deposited polyaniline films. J Electrochem Chem 1996;412:133–7.
[26] Duic L, Mandic Z, Kovac S. Polymer-dimer distribution in the electrochemical synthesis of polyaniline. Electrochim Acta 1995;40(11):1681–8.
[27] Feigin LA, Svergun DI. Structure analysis by small-angle X-ray and neutron scattering. New York: Plenum Press; 1987. p. 88.
[28] Nishikawa K. Pore structure analyses of carbons by small-angle X-ray scattering. In: Yasuda E, Inagaki M, Kaneko K, et al. editors. Carbon Alloys. Oxford: Elsevier Sci. Ltd.; 2003. p. 181–2.
[29] Takei T, Dong Q, Yonesaki Y, Kumada N, Kinomura N. Preparation of hybrid film of polyaniline and organically pillared zirconium phosphate nanosheet by electrodeposition. Langmuir 2011;27(1):126–31.
[30] Guinier A, Fournet G, Walker CB. Small angle scattering of X-rays. New York: Wiley; 1955. p. 5–78.